


Spectrum Reconstruction of a Spatially Modulated Fourier Transform Spectrometer Based on Stepped Mirrors

Jianhua Gao^{1,2}, Zhongzhu Liang¹, Jingqiu Liang¹, Weibiao Wang¹,
Jinguang Lü¹, and Yuxin Qin¹

Applied Spectroscopy
2017, Vol. 71(6) 1348–1356
© The Author(s) 2016
Reprints and permissions:
sagepub.co.uk/journalsPermissions.nav
DOI: 10.1177/0003702816669729
journals.sagepub.com/home/asp


Abstract

Based on the basic configuration and interference principle of a static step-mirror-based Fourier transform spectrometer, an image segmentation method is proposed to obtain a one-dimensional interferogram. The direct current component of the interferogram is fit using the least squares (LS) method and is subsequently removed. An empirical-mode decomposition-method-based high-pass filter is constructed to denoise the spectrum and enhance the spectral resolution simultaneously. Several experiments were performed and the spectrum is reconstructed based on these methods. The spectrum resolution is 81 cm^{-1} at 2254 cm^{-1} .

Keywords

Step mirror, Fourier transform (FT) spectrometer, image segmentation, spectrum reconstruction, empirical-mode decomposition denoising

Date received: 29 May 2016; accepted: 16 August 2016

Introduction

Fourier transform (FT) spectrometry is widely used in many fields,^{1–5} such as material component analysis, environmental monitoring, life sciences, and modern medicine, owing to its advantages, such as multiple channels, highly luminous flux, high stability, high signal-to-noise (S/N) ratio, and long operation life.⁶ The classical FT spectrometer is generally based on the Michelson spectrometer and is temporally modulated.^{6–8} It has a motion control system that positions a moving mirror to achieve the desired optical path differences (OPDs). To guarantee the accuracy of the OPDs, the motion control system must be very precise, which not only increases the cost and bulk of the device but also decreases its stability.

To eliminate the influence of the precise motion system on the FT spectrometer, researchers proposed spatially modulated spectrometers. In 1992, Möller et al. first proposed the step-mirror-based spectrometer⁹ and later his co-workers studied its resolving power and applications.^{10–12} Möller's spectrometer realized the goal of a static interference system. To achieve a miniaturized and lightweight FT spectrometer, Liang et al. proposed a step-mirror-based FT spectrometer (SMFTS) and studied the effect of diffraction, the design, and fabrication of lower and higher step mirrors, etc.^{13–18} The core components

of SMFTS are two step mirrors fabricated by micro-optical electromechanical system (MOEMS) technology. The interferogram of SMFTS is different from that of the classical one because of the special configuration of the step mirrors and the novel data processing and spectrum reconstruction methods, which were developed.

Step-Mirror-Based Fourier Transform Spectrometry

Figure 1 shows a simplified configuration of the SMFTS. It is composed of a light source, collimating system, sample compartment, beam splitter, compensating plate, higher step mirror, lower step mirror, expansion system, and detector array. Its interference system is based on the Michelson interferometer, but with two vertically placed

¹State Key Laboratory of Applied Optics, Changchun Institute of Optics, Fine Mechanics and Physics, Chinese Academy of Sciences, Changchun, Jilin, China

²University of Chinese Academy of Sciences, Beijing, China

Corresponding author:

Zhongzhu Liang, State Key Laboratory of Applied Optics, Changchun Institute of Optics, Fine Mechanics and Physics, Chinese Academy of Sciences, Changchun, Jilin 130033, China.
Email: liangzz@ciomp.ac.cn

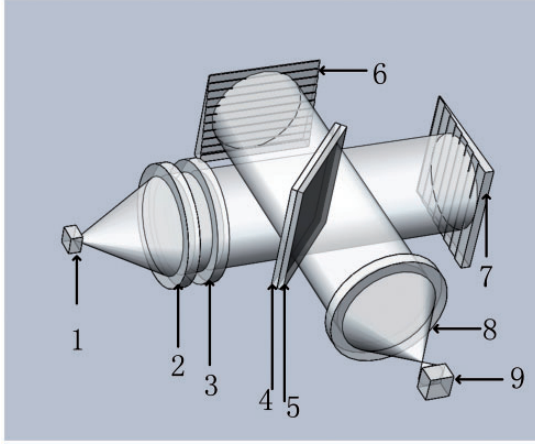


Figure 1. Simplified configuration of the SMFTS: (1) light source, (2) collimating system, (3) sample compartment, (4) beam splitter, (5) compensating plate, (6) higher step mirror, (7) lower step mirror, (8) expansion system, and (9) detector array.

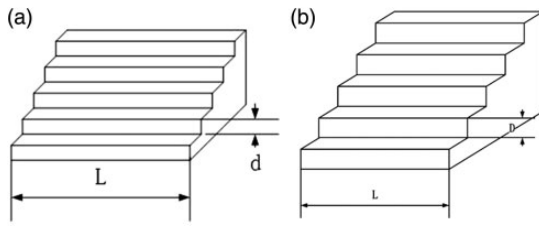


Figure 2. Sketch of lower and higher step mirrors.

step mirrors substituting the moving and static mirrors in the classical device. This substitution makes the interference process static.

Radiation emitted from the light source propagates through the sample compartment and collimating system to the beam splitter. The beam splitter then divides the incident light into two beams. One beam is reflected towards one of the step mirrors and the other is transmitted to the other step mirror. The two beams of light are reflected back by the two step mirrors and propagate through the expansion system to finally reach to the detector array and form the interferogram.

Interference Principles

As shown in Figure 2, the height of the lower step mirror is d and the height of the higher step mirror is D . Each step mirror has M steps. The positions of the two step mirrors are adjusted to make one of the OPDs zero so that the space sampling interval is $2d$. Let the light wavelength range be $[\lambda_{\min}, \lambda_{\max}]$, where λ_{\min} and λ_{\max} indicate the minimum and maximum wavelengths that can be detected by the detector array, respectively. According to the Nyquist–

	j		$j+m$	
i		$\delta(0,0)$		$\delta(0,m)$
			.	
$i+n$.	
			.	
		$\delta(n,0)$		$\delta(n,m)$

Figure 3. Optical path difference distribution at the detector array.

Shannon criterion, the sampling frequency f_s should satisfy $f_s \geq 2f_{\max}$. The spatial sampling interval should therefore satisfy $2d \leq \lambda_{\min}/2$, which means the height of one step of the lower step mirror should be equal to or less than $\lambda_{\min}/4$. To obtain successive OPDs, the total height of the lower step mirror should be equal to the height of one step of the higher step mirror, i.e., $D = M \times d$. Suppose the OPD between the i th step of higher step mirror and the j th step of the lower step mirror is $\delta(i,j) = 0$. This means the OPD between the $(i+m)$ th step of higher step mirror and the $(j+n)$ th step of the lower step mirror is $\delta(i+m, j+n) = 2 \times (m \times D - n \times d)$. Let us substitute $\delta(i+m, j+n)$ with $\delta(m, n)$ so that the OPDs at the detector array's plane can be set as shown in Figure 3.

Data-Processing Principles

For an FT spectrometer, the relationship between the interferogram and spectrum is:

$$B(\sigma) = F\{I(\delta) - I_{dc}\} = \int_{-\infty}^{\infty} [I(\delta) - I_{dc}] e^{-i2\pi\sigma\delta} d\delta \quad (1)$$

where $B(\sigma)$ is the spectrum, $I(\delta)$ is the interferogram, I_{dc} is the direct current (DC) part of interferogram, and F indicates the Fourier transformation.

Because they are affected by the lens fabrication accuracy, mechanical component accuracy, jitter, background noise, etc., experimental interferograms often contain background noise, distortion, phase errors, and so on. Thus, an interferogram should be preprocessed before spectral reconstruction. The preprocessing procedure includes image division and dimension reduction, DC offset removal, interferogram addressing, apodization, and

phase correction. After the spectrum is reconstructed, we applied the empirical-mode decomposition (EMD)-based denoising method to reduce the noise level of the spectrum and enhance the resolution.

Image Division and Dimension Reduction. Operation of the spectrometer provides a two-dimensional (2D) interferogram, which should be transformed to a one-dimensional (1D) interferogram for reconstructing the spectrum. After defining the area that has the same OPD as an interferogram unit and assuming the size of the interferogram matrix is $N \times N$, one interferogram unit at the expansion system is collected by $n \times n$ pixels in the detector array. Therefore, we can divide the interferogram into $M \times M$ blocks, where $M = N/n$. The block size is approximately $n \times n$, and each block corresponds to a certain OPD.

According to the principle of SMFTS, each interferogram unit corresponds to a certain OPD and different OPDs correspond to different light intensities, which means that edges between different units are clearly differentiable. The various zones of OPDs could be determined by the geometry of the step mirrors and the imaging of the aperture on

the detector. However, because of the fabrication accuracy of the step mirrors and the optical system alignment errors, the zones may not always accurate. Therefore, we applied the Canny method to refine the edge locations with respect to the predicted edge locations.¹⁹ Canny edge detection can be used to find the edges of each unit because it can detect both horizontal and vertical edges and suppress noise to detect weak edges. The result of the edge detection could be used to accomplish the image division.

There may be some parts of the image that cannot be divided properly. We can handle this problem by isolating these parts and detecting the edges of each part separately using the Canny method with different threshold values. Finally, we can combine these results to obtain accurate division for the whole interferogram.

For the purpose of suppressing random noise, we can choose the median value of the area as its new value. Arranging the median values in order of OPDs produces a 1D interferogram.

Suppose I is the interferogram. The image division and dimension reduction process can be expressed as Eq. 2 to Eq. 5:

$$\begin{pmatrix} I_{11} & \cdots & I_{1n} & \cdots & I_{1(N-n+1)} & \cdots & I_{1N} \\ \vdots & \ddots & \vdots & \ddots & \vdots & \ddots & \vdots \\ I_{n1} & \cdots & I_{nn} & \cdots & I_{n(N-n+1)} & \cdots & I_{nN} \\ \vdots & \ddots & \vdots & \ddots & \vdots & \ddots & \vdots \\ I_{(N-n+1)1} & \cdots & I_{(N-n+1)n} & \cdots & I_{(N-n+1)(N-n+1)} & \cdots & I_{(N-n+1)N} \\ \vdots & \ddots & \vdots & \ddots & \vdots & \ddots & \vdots \\ I_{N1} & \cdots & I_{Nn} & \cdots & I_{N(N-n+1)} & \cdots & I_{NN} \end{pmatrix} \quad (2)$$

$$\begin{pmatrix} I_{11} & \cdots & I_{1n} & \cdots & I_{1(N-n+1)} & \cdots & I_{1N} \\ \vdots & \ddots & \vdots & \ddots & \vdots & \ddots & \vdots \\ I_{n1} & \cdots & I_{nn} & \cdots & I_{n(N-n+1)} & \cdots & I_{nN} \\ \hline \vdots & & \vdots & \ddots & \vdots & & \vdots \\ \hline I_{(N-n+1)1} & \cdots & I_{(N-n+1)n} & \cdots & I_{(N-n+1)(N-n+1)} & \cdots & I_{(N-n+1)N} \\ \vdots & \ddots & \vdots & \ddots & \vdots & \ddots & \vdots \\ I_{N1} & \cdots & I_{Nn} & \cdots & I_{N(N-n+1)} & \cdots & I_{NN} \end{pmatrix} \quad (3)$$

$$\begin{pmatrix} I'_{11} & \cdots & I'_{1M} \\ \vdots & \ddots & \vdots \\ I'_{M1} & \cdots & I'_{MM} \end{pmatrix} \quad (4)$$

$$(I'_{11}I'_{21}\cdots I'_{M1}I'_{12}I'_{22}\cdots I'_{M2}\cdots I'_{MM}) \quad (5)$$

where $I'_{ij} = \text{median}(I_{ij})$, I_{ij} indicates one interferogram unit of I , and median means the median value function.

Direct Current Offset Removal. Light intensity collected by the detector array is the superposition of a DC offset, which has a constant value, and an alternating current (AC) offset, which has a changing value and determines the shape of the spectrum. Classical DC offset removal uses the 1D interferogram minus its mean value to obtain the AC part. However, in practice, the DC offset is not always a constant value but varies erratically with OPD because of jitter, fabrication error of step mirrors, stability of light source, etc. Therefore, simple subtraction of the mean value is not enough to remove the entire DC offset of the 1D interferogram. To obtain a satisfactory result, we should fit the interferogram to find different DC values at each position and then subtract those values. The DC offset removal process can be described as Eq. 6:

$$I_{ac} = I' - I_{dc} \quad (6)$$

where I_{ac} and I_{dc} are the AC offset and DC offset of the interferogram, respectively. I' is the 1D interferogram.

Interferogram Addressing. The purpose of the addressing process is to find the maximum value I_{\max} of I_{ac} and use it as the light intensity value of the interferogram at zero OPD (ZPD). The address of I_{\max} is used as the axis origin and other coordinates of the interferogram are arranged according to it. More specifically, the sample points to the right of I_{\max} correspond to OPDs: $\Delta, 2\Delta, L$, and the sample points to the left of I_{\max} correspond to OPDs: $-1\Delta, -2\Delta, L$, where Δ is the sampling interval.

Interferogram Apodization. As described in Griffiths and De Haseth,¹⁹ the effect of the apodization is to modify the ILS in particular to trade spectral resolution against oscillation in the line shape. The apodization process can be expressed as:

$$I_{apo} = I_{ac} \times I_{dc} \quad (7)$$

where I_{ac} is rearranged AC offset of the interferogram and Win is the window function.

Interferogram Phase Correction. The first step of the phase correction procedure is to correct the non-uniform sampling caused by the height error of the higher and lower

Table 1. Step mirror height test results.

	Maximum	Minimum	Mean	Variance
Lower/nm	0.840	0.546	0.625	0.005
Higher/ μm	22.375	16.500	20.251	1.116

step mirrors. The FT require uniform OPD interval between various sample points to guarantee the accuracy of the reconstructed spectra. In the first instance, the uniformity of the OPD interval is determined by the precision of manufacturing of the step mirrors and the optics and of the interferometer. Table 1 shows the height test result of the step mirrors.

As we can see in Table 1, the height of lower and higher step mirrors drifted from the ideal value, which makes the sampling interval non-uniform. The maximal drift of the lower and higher step mirrors are 34.4% and 17.5%, respectively. According to Hirschfeld,²¹ the theoretical maximum S/N ratio relates to the sampling errors:

$$SNR_{\max} = \frac{4}{\Delta x \tilde{\nu}_{\max}} \quad (8)$$

where Δx is the root mean square error (RMSE) of the sampling interval, $\tilde{\nu}_{\max}$ is the maximum wavenumber of the source. To achieve an S/N ratio higher than 1000 in the mid-infrared (IR) ($\tilde{\nu}_{\max} = 4000 \text{ cm}^{-1}$), Δx should be less than 10 nm, which is beyond the fabrication accuracy of the step mirrors. This means the sampling interval between different points may not be uniform. The fabrication errors will add residual errors to OPD and consequently limit the obtainable spectral precision.

The ways to deal with this problem contain interpolation, non-uniform discrete FT, etc. Because the sampling interval error could be calculated from the tested step height, the interpolation method is used to correct the non-uniformity.

The ideal OPD distribution is shown in Figure 3. We define the height error as the tested value minus the ideal one and one assumes that the height errors of the $(i+m)$ th step of the higher step mirror and the $(j+n)$ th step of the lower step mirror is $H\Delta_{i+m}$ and $h\Delta_{j+n}$, respectively. As discussed above, the OPD error between the two steps should be:

$$\delta E(i+m, j+n) = 2 \times [m \times H\Delta_{i+m} - n \times h\Delta_{j+n}] \quad (9)$$

Assuming that δR_i ($i = 1, 2, \dots, N$) is the real OPD distribution, δE_i ($i = 1, 2, \dots, N$) is the error matrix, and δI_i ($i = 1, 2, \dots, N$) is the ideal OPD distribution, the correction details are as follows:

1. Test the step height of the lower and higher step mirrors, calculate the height deviation to the designed value of each step;

2. Calculate the error matrix δE_i using Eq. 9;

$$\delta R_i = \delta I_i - \delta E_i \quad (10)$$

4. Once δR_i is obtained, the residual sampling error is corrected using an interpolation method.

The sampling position may drift from the ideal value due to jitter and adjustment error of the optical system. This introduces random phase errors to the interferogram. Suppose the interferogram drifts δ_0 from ideal position, so

$$B(\sigma) = \int_{-\infty}^{\infty} (I(\delta - \delta_0) - I_{dc}) e^{-i2\pi\sigma\delta} d\delta \quad (11)$$

To decrease the influence of δ_0 on the reconstructed spectrum, phase correction should be performed before the discrete FT. Many methods, such as the Forman, Mertz, and Connes methods have been developed to realize phase correction.^{23–25} Among these methods, the Connes method critically requires symmetric double-sided sampling data to decrease the phase error. The Mertz method operates in the spatial domain and is easy to compute. The Forman method operates in the space domain and effectively corrects both linear and non-linear phase errors. The Mertz method is more computationally efficient compared to the Forman methods due to the high computational requirements of convolution in the Forman method. However, if single-sided interferograms are collected, which is done in our experiments, the error in the Mertz method can be significant, as the error can be greater than 1% transmission.²⁶ To guarantee the accuracy of the reconstructed spectra, the Forman method was chosen for phase correction.

The main idea behind the Forman method is to construct a phase function by utilizing the symmetrical short double-sided interferogram, and then using the inverse FT of this function to correct the longer interferogram that is used to obtain the spectrum. In detail:

1. Obtain the short double-sided interferogram;
2. Shift the short double-sided interferogram and perform a FT

$$B_d(\sigma) = F\{I_d(\delta)\} \quad (12)$$

where $I_d(\delta)$ is the short double-sided interferogram. After the FT, we can calculate the phase error as:

$$\varphi(v) = -\arctan \frac{\text{Im}(v)}{\text{Re}(v)} \quad (13)$$

where $\text{Im}(v)$ and $\text{Re}(v)$ are the imaginary and real parts of $B_d(\sigma)$, respectively.

3. Construct the phase function and perform an inverse FT

$$f_p = \exp[i\varphi(v)] \quad (14)$$

where f_p is the phase function and $\varphi(v)$ is the phase error.

$$I'_d(\delta) = F^{-1}\{f_p\} \quad (15)$$

where $I'_d(\delta)$ is the inverse FT of f_p .

4. Perform the interferogram phase correction

$$I'(\delta) = I(\delta) * I'_d(\delta) \quad (16)$$

where $I'(\delta)$ is the corrected interferogram, $I(\delta)$ is the original 1D interferogram, and $*$ indicates convolution.

Empirical-Mode Decomposition Denoising Algorithm. Although we implied a denoising method above, a certain amount of noise still remains in the signal. An EMD-based filter is constructed to deal with the remaining noise. The EMD was first proposed by Huang et al. at NASA²⁶ and was widely used in many fields.^{28–31} It is a data-driven method that could be used to deal with non-stationary and non-linear signals because its advantages of adaptively decomposing a signal to different frequencies and high time-frequency resolution.

The EMD method decomposes the signal to intrinsic mode functions (IMF) by the shifting process (SP) method. The IMF is identified by two characteristics: (1) the number of extrema and the number of zero crossings either be equal or differ at most by one in the whole data set; and (2) the mean value of the upper envelope defined by the local maxima and the lower envelope defined by the local minima should be equal to zero.²²

$$X(t) = \sum_{j=1}^n c_j(t) + r_n(t) \quad (17)$$

where, $X(t)$ is the reconstructed signal, $c_j(t)$ is the intrinsic mode function obtained by applying the EMD, and $r_n(t)$ is the monotonic residue.

The spectral information is mainly contained in the sudden change part, which corresponds to high frequency. We proposed a high-pass filter based on the EMD result because the EMD has the ability to decompose signals to different frequencies.

The direct way to design a high-pass filter is to reserve some of the low order IMFs, which correspond to the high frequencies, and throw the others away. However, this would lead to information loss because the low frequency

parts also carry some information. Therefore, the method we proposed uses all the IFMs to reconstruct the signal, but the weights of the IFMs are changed.

$$X(t) = \sum_{j=1}^n a_j c_j(t) + r'_n(t) \quad (18)$$

where a_j is the coefficient of $c_j(t)$, and $r'_n(t)$ is the residue.

The coefficient may be obtained by the process below:

1. Get the maximum value M_j of each IMF_j , and calculate their algebraic sum S ;
2. Calculate the initial coefficient b_j using Eq. 19:

$$b_j = \frac{M_j}{S} \quad (19)$$

3. Calculate a_j using Eq. 20:

$$a_j = \begin{cases} b_1 + \Delta & j = 1 \\ \frac{b_j}{j^3} & j = 2, 3, \dots, n \end{cases} \quad (20)$$

where $\Delta = \text{sum}(b_j - a_j), j = 2, 3, \dots, n$, *sum* means the algebraic sum.

Once a_j is obtained, we can reconstruct the signal using Eq. 18 and then calculate the root mean square error (RMSE) using Eq. 21 to see whether the method is effective or not.

$$RMSE = \left\{ \frac{1}{N} \sum_{j=1}^N [x(j) - \hat{x}(j)]^2 \right\}^{\frac{1}{2}} \quad (21)$$

where $x(j)$ is the original signal, $\hat{x}(j)$ is the denoised signal, and N is the length of the signal.

Experimental Results and Analysis. Figure 4 shows the prototype of SMFTS, and several experiments have been performed with it to obtain the spectrum of acetonitrile (CH₃CN), which has an absorption peak at 2254 cm^{-1} .^{17,32} A SiC IR light source was used. The step differences for the higher step mirror and the lower step mirror are $20 \mu\text{m}$ and $0.625 \mu\text{m}$, respectively. The sample interval is $1.25 \mu\text{m}$. The detector is a mercury–cadmium–telluride (MCT) mid-IR focal-plane detector array that contains 320×256 pixels with a pixel size of $30 \times 30 \mu\text{m}$.

According to FT spectrometer practice, two interferograms are required: one with an empty sample compartment and the other with the sample present. The absorption interferogram of the sample can be obtained by using the difference between the interferogram without

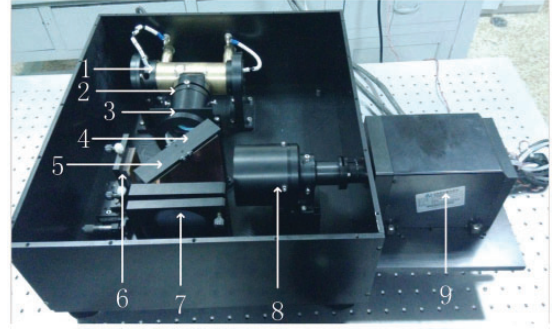


Figure 4. Prototype of the SMFTS: (1) light source, (2) collimating system, (3) sample compartment, (4) beam splitter, (5) compensating plate, (6) higher step mirror, (7) lower step mirror, (8) expansion system, and (9) detector array.

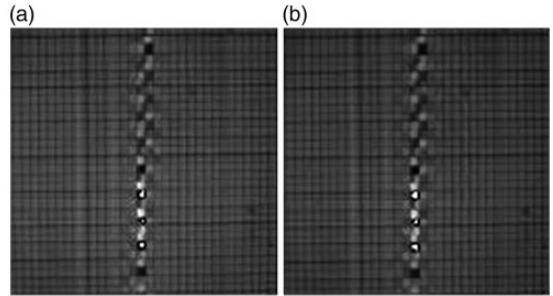


Figure 5. Interferogram with no sample (a) and with sample (b).

the sample and the interferogram with the sample. The images are shown in Figure 5.

Using the Canny method described above, the 2D interferogram is divided into blocks. Figure 6a shows the 1D interferogram after image segmentation, as we can see, it is not exactly symmetric and the base line is curved, which means the DC offset changes with OPD in a non-linear way.

To deal with the asymmetrical problem, we applied the LS fitting method to estimate the correct baseline and used it to perform the baseline correction. The results are shown in Figure 6a and b. Figure 6b is more symmetrical than Figure 6a and the corrected base line is almost equal to zero.

After baseline correction, the interferogram is arranged in OPD order and the result is shown in Figure 6c.

In the apodization procedure, the Happ–Genzel function expressed in Eq. 22 is selected as the apodization function.³¹

$$D(\delta) = 0.54 + \cos(\pi\delta/\Delta_{\max}) \quad (22)$$

where Δ_{\max} indicates the maximum OPD. The apodization result is shown in Figure 6d.

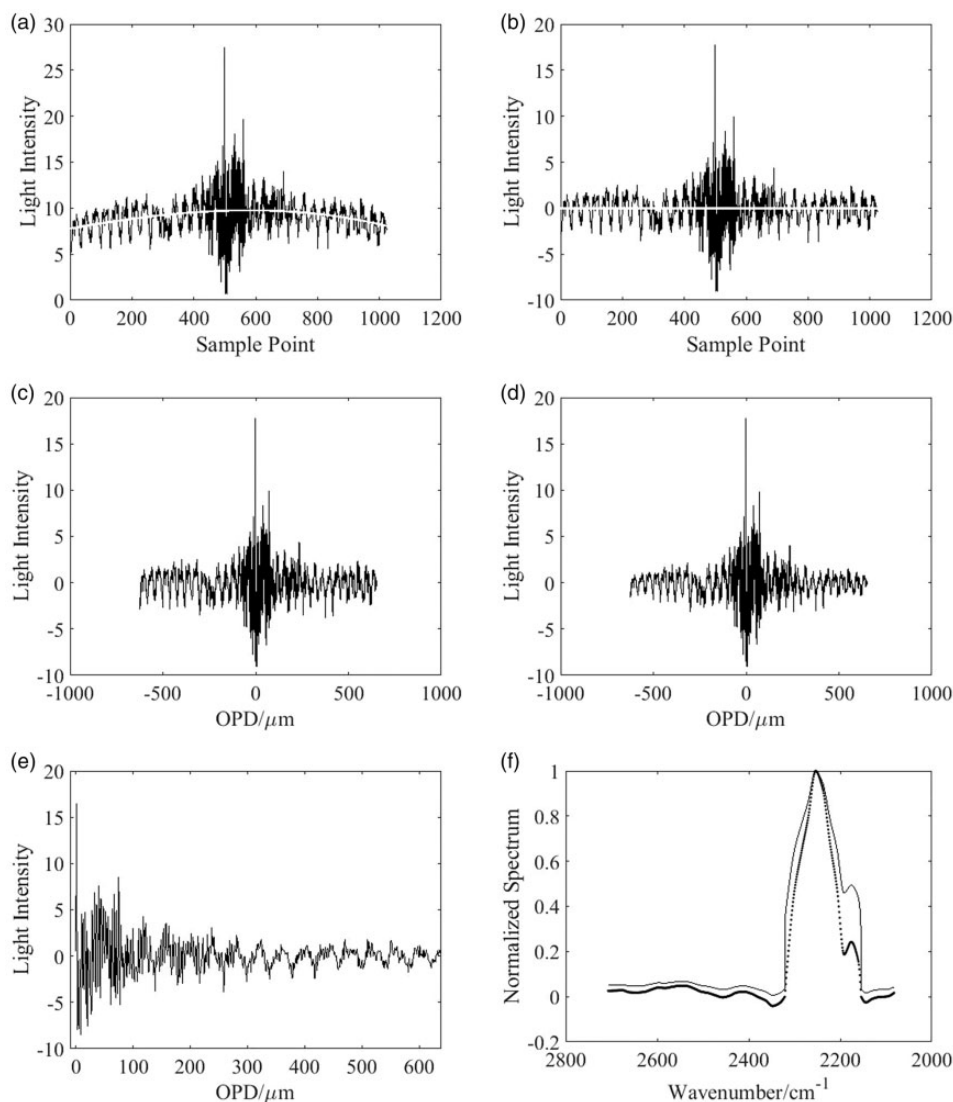


Figure 6. (a) One-dimensional interferogram and its baseline (white line); (b) interferogram after DC offset removal and its base line (white line); (c) interferogram addressed in OPD order; and (d) interferogram after apodization. The apodization Happ–Genzel function (e) and interferogram after phase correction with Forman method; (f) normalized spectrum before and after denoising.

Several experiments were performed with a narrow-band filter, which has a band width of 6 cm^{-1} at 2347 cm^{-1} . The result is shown in Figure 7. The spectrum resolution (full width at half height) is 81 cm^{-1} .

A short double-sided interferogram containing 128 points on each side of the ZPD was chosen and the points used for the discrete FT were corrected by utilizing these points. The phase correction result is shown in Figure 6e.

Figure 6f shows the normalized spectrum before and after denoising (dotted line). As we can see in Figure 11, the spectrum after denoising has lower slopes than before and the spectral resolution is enhanced by 35 cm^{-1} .

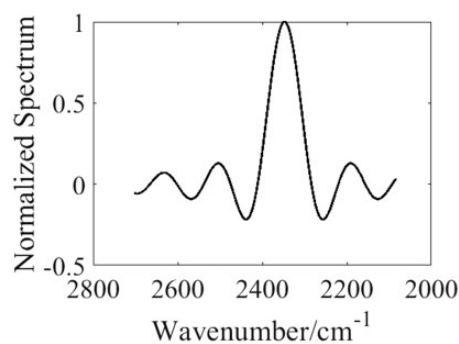


Figure 7. Instrument line-shape function.

The RMSE of the spectrum is less than 0.29. The spectrum resolution is 81 cm^{-1} at 2254 cm^{-1} .

Conclusion

The step mirrors, which are the key components of the SMFTS, make the OPD distribution unique, and an image segmentation method is proposed to handle this. One-dimensional interferograms were obtained with the help of this method. The interferogram base line is almost equal to zero after correction using LS fitting; phase correction is done by the Forman method. Although the spectrum resolution is not satisfactory for many applications, the absorption band due to the CN stretching mode of the acetonitrile spectrum was obtained.

The EMD-based high-pass filter is proposed to denoise the signals of the SMFTS and enhance the spectral resolution. It is a data-driven method and has the desirable characteristic of adaptive signal processing. This method is suitable for other signals which have sharp peaks. If a signal has more than one peak, we can break them into some sub-sections before EMD and combine them together after reconstruction.

Conflict of Interest

The authors report there are no conflicts of interest.

Funding

The authors gratefully acknowledge the support of the National Natural Science Foundation of China (61575193, 61376122, 61027010, 61627819), Science and Technology Development Plan of Jilin Province (20150520101JH, 20150101049JC, 20150204072GX, 20130206010GX), Changchun Science Development Plan (2013261), and State Key Laboratory of Applied Optics, Changchun Institute of Optics, Fine Mechanics and Physics, Chinese Academy of Sciences.

References

1. R.B. Horton, E. Duranty, M. McConico, F. Vogt. "Fourier Transform Infrared (FT-IR) Spectroscopy and Improved Principal Component Regression (PCR) for Quantification of Solid Analytes in Microalgae and Bacteria". *Appl. Spectrosc.* 2011. 65(4): 442–453.
2. G. Parodi, P. Dickerson, J. Cloud. "Pollen Identification by Fourier Transform Infrared Photoacoustic Spectroscopy". *Appl. Spectrosc.* 2013. 67(3): 342–348.
3. M. Picollo, G. Bartolozzi, C. Cucci, M. Galeotti, V. Marchiafava, B. Pizzo. "Comparative study of Fourier transform Infrared Spectroscopy in Transmission, Attenuated Total Reflection, and Total Reflection Modes for the Analysis of Plastics in the Cultural Heritage Field". *Appl. Spectrosc.* 2014. 68(4): 389–397.
4. O.F. Sarioglu, Y.T. Tamer, A.D. Ozkan, H.I. Atabay, C. Molva, T. Tekinay. "Fourier Transform Infrared Spectroscopy as a Novel Approach for Analyzing the Biochemical Effects of Anionic Surfactants on a Surfactant-Degrading *Arcobacter Butzleri* Strain". *Appl. Spectrosc.* 2013. 67(4): 470–475.
5. T. Zhang, L. Wan, Y. Yuan, Y. Duan, J. Zhang. "Chemical Structure and Interlayer Distance Correlation of Graphite Oxide in the Heating Process as Revealed by in situ Fourier Transform Infrared Spectroscopy and Wide-Angle X-ray Diffraction Techniques". *Appl. Spectrosc.* 2014. 68(5): 570–576.
6. V. Saptari. "Spectroscopy Instrumentation". In: A.R. Weeks (ed.) *Fourier-Transform Spectroscopy Instrumentation Engineering*, 1st ed. Bellingham, WA: SPIE, 2003Chap. 1, Pp. 3–6.
7. K. Yu, D. Lee, U. Krishnamoorthy, N. Park, O. Solgaard. "Micromachined Fourier Transform Spectrometer on Silicon Optical Bench Platform". *Sens. Actuators, A*. 2006. 130: 523–530.
8. D. Reyes, E.R. Schildkraut, J. Kim, R.F. Conners, P. Kotidis, D.J. Cavicchio. "A Novel Method of Creating a Surface Micromachined 3D Optical Assembly for MEMS-Based Miniaturized FTIR Spectrometers". *Proc. SPIE 6888, MEMS Adaptive Optics II*. 2008. 68880D.
9. K.D. Moeller. "Miniaturized Wavefront-Dividing Interferometers without Moving Parts for Field and Space Applications". *Proc. SPIE, Miniature and Micro-Optics and Micromechanics*. 1993. 130http://dx.doi.org/10.1117/12.165681.
10. A. Lacan, F.M. Bréon, A. Rosak, F. Brachet, L. Roucayrol, P. Etcheto, C. Casteras, Y. Salaun. "A Static Fourier Transform Spectrometer for Atmospheric Sounding: Concept and Experimental Implementation". *Opt. Express*. 2010. 18(8): 8311–8331.
11. F. Brachet, P.J. Hébert, E. Cansot, et al. "Static Fourier Transform Spectroscopy Breadboards for Atmospheric Chemistry and Climate". *Proc. SPIE 7100, Optical Design and Engineering III*. 710019 (27 September 2008). doi: 10.1117/12.797686.
12. E.V. Ivanov. "Static Fourier Transform Spectroscopy with Enhanced Resolving Power". *J. Opt. A: Pure Appl. Opt.* 2000. 2(6): 519.
13. Y. Zheng, J.Q. Liang, Z.Z. Liang. "Design and Fabrication of Step Mirrors used in Space-Modulated Fourier Transform Infrared Spectrometer". *Opt. Express*. 2013. 21(1): 884–892.
14. J.G. Lu, J.Q. Liang, Z.Z. Liang, Y.X. Qin, C. Tian, W.B. Wang. "Design and Manufacture of Micro Interference System in Spatial Modulation Fourier Transform Spectrometer". *Key Engineering Materials*. 2013. 562: 973–978.
15. C. Chen, J.Q. Liang, Z.Z. Liang, J. Lu, Y. Qin, C. Tian, W. Wang. "Fabrication and Analysis of Tall-Stepped Mirror for use in Static Fourier Transform Infrared Spectrometer". *Opt. Laser. Technol.* 2015. 75: 6–12.
16. C. Feng, B. Wang, Z.Z. Liang, J. Liang. "Miniaturization of Step Mirrors in a Static Fourier Transform Spectrometer: Theory and Simulation". *J. Opt. Soc. Am. B*. 2011. 28(1): 128–133.
17. J.Q. Liang, Z.Z. Liang, J.G. Lu, J.G. Fu, Y. Zheng, C. Feng, W.B. Wang, W.B. Zhu, J.S. Yao, J. Zhang. "Simulation and Experiment of the Static FTIR based on Micro Multi-Step Mirrors". *Proc. SPIE 8191, International Symposium on Photoelectronic Detection and Imaging 2011. International Society for Optics and Photonics*. 2011. 819104–819104-8.
18. C. Feng, J.Q. Liang, Z.Z. Liang. "Spectrum Constructing with Nonuniform Samples Using Least-Squares Approximation by Cosine Polynomials". *Appl. Opt.* 2011. 50(34): 6377–6383.
19. R.C. Gonzalez, R.E. Woods, S.L. Eddins. "Image Segmentation". In: R. Qiuqi (ed.) *Digital Image Processing Using MATLAB*, 2nd ed. Publication house of electronics industry, 2013, Chap. 7, Pp. 209–211.
20. P.R. Griffiths, J.A. de Haseth. "Theoretical Background". In: P.R. Griffiths, J.A. de Haseth (eds) *Fourier Transform Infrared Spectrometry*, 2nd ed. Hoboken, NJ: John Wiley & Sons, 2007, Chap. 2, Pp. 26–30.
21. T. Hirschfeld. "Quantitative FT-IR: A detailed look at the problems involved". In: J.R. Ferraro and L.J. Basile (eds) *Fourier Transform Infrared Spectroscopy: Application to Chemical Systems*. Vol. 2, New York, NY: Academic Press, 1979, Pp. 193–242.
22. B. Xiangli, Q. Lu, M. Huang. "Advance in Interferogram Data Processing Technique". *Guang Pu Xue Yu Guang Pu Fen Xi [Spectrosc. Spect. Anal.]*. 2011. 31(4): 865–870.
23. R. Furstenberg, J.O. White. "Phase Correction of Interferograms Using Digital All-Pass Filters". *Appl. Spectrosc.* 2005. 59(3): 316–321.

24. M.J. Zhang, J.L. Zhang, Z.B. Wang, N. Jing, J. Hao. "Phase Correction Technology Research and Improvement Based on Single-Sided Interferograms in FTIR". *Guang Pu Xue Yu Guang Pu Fen Xi [Spectrosc. Spect. Anal.]*. 2012. 32(5): 1203–1208.
25. P.R. Griffiths, J.A. De Haseth. "Fourier Transforms". In: P.R. Griffiths, J.A. de Haseth (eds) *Fourier Transform Infrared Spectrometry*, 2nd ed. Hoboken, NJ: John Wiley & Sons, 2007Chap. 7, Pp. 85–88.
26. N.E. Huang, Z. Shen, S.R. Long, M.C. Wu, H.H. Shih, Q. Zheng, N.-C. Yen, C.C. Tung, H.H. Liu. "The Empirical Mode Decomposition and the Hilbert Spectrum for Nonlinear and Non-Stationary Time Series Analysis". *Proc. R. Soc. London, Ser. A*. 1998. 454(1971): 903–995.
27. E. Deléclle, J. Lemoine, O. Niang. "Empirical Mode Decomposition: An Analytical Approach for Sifting Process". *IEEE Signal. Proc. Let.* 2005. 12(11): 764–767.
28. C.H. Hsu, C.Y. Lee, W.K. Liang. "An Improved Method for Measuring Mismatch Negativity Using Ensemble Empirical Mode Decomposition". *J. Neurosci. Meth.* 2016. 264: 78–85.
29. Y. Yang. "Empirical Mode Decomposition as a Time-Varying Multirate Signal Processing System". *Mech. Syst. Signal. Pr.* 2016. 76: 759–770.
30. F. Zhou, L. Yang, H. Zhou, L. Yang. "Optimal Averages for Nonlinear Signal Decompositions: Another Alternative for Empirical Mode Decomposition". *Signal Process.* 2016. 121(C): 17–29.
31. C. Chen. *Optical Design and Core Components Study for Static Fourier Transform Infrared Spectrometer*. University of Chinese Academy of Sciences, [Ph.D. dissertation]. 2016. Chap. 7, Pp. 117–125.